Yaw induced wake deflection - a full-scale validation study

Larsen, G.C.; Ott, S.; Liew, J.; van der Laan, M.P.; Simon, E.; R.Thorsen, G.; Jacobs, P.

Published in:
Journal of Physics - Conference Series

Link to article, DOI:
10.1088/1742-6596/1618/6/062047

Publication date:
2020

Document Version
Peer reviewed version

Yaw induced wake deflection - a full-scale validation study

G.C. Larsen[1], S. Ott[1], J. Liew[1], M.P. van der Laan[1], E. Simon[1], G.R. Thorsen[1] and P. Jacobs[1]

[1]Department of Wind Energy, Technical University of Denmark (DTU), Frederiksborgvej 399, 4000 Roskilde, Denmark

E-mail: gula@dtu.dk

Abstract. Aerodynamic wake interactions between turbines located in wind power plants cause both a loss in power production and an increase in fatigue loading of the wind farm turbines. Yaw induced active wake deflection is one possible wind farm control strategy, which can be applied to mitigate wake effects on nearby downstream located wind turbines. In the present study three flow models of different fidelities are applied to mimic a full-scale study of wake deflection recorded by an advanced synchronised setup of two long-range pulsed scanning lidars. The investigated case studies encompass a base case with (approximately) zero yaw setting supplemented by two non-zero yaw cases of 17.5° and -14.5°, respectively. The model results are compared mutually as well as with the result of the full-scale measurement campaign.

1. Introduction

Aerodynamic wake interactions between turbines located in wind power plants (WPPs) can cause both a loss in power production and an increase in fatigue loading. To mitigate such effects there is a growing interest in (optimal) WPP control strategies within the wind energy community during recent years. Such strategies are based on *active wake control* (AWC), which basically falls in two disjunct classes - 1) wind turbine (WT) de-rating and 2) lateral wake displacement obtained by yawing the wake generating wind turbines (WTs) on purpose.

WT de-rating is characterized by operating selected WTs in a WPP with sub-optimal set-points, by which the power production sacrifice of these selected WTs allows for optimizing the power production of the WPP as a whole [1]. An analog philosophy is true for active yaw control [2]. Here, the basic idea is to operate selected WPP WTs sub-optimally by yawing these WTs by purpose and thereby, to a certain degree, facilitating the lateral deflection of downstream wake patterns with the purpose of avoiding or mitigating wake influence on nearby downstream located WTs.

A recent review study by Kheirabadi et al. [3] indicates a huge scatter among simulated high-fidelity-, medium-fidelity- and low-fidelity model predictions of the potential WPP AWC efficiency gains, and thereby in turn questions the reliability of such estimates. In addition, it is also reported that field tests seem to provide the most conservative evaluations due to the *stochastic time-varying nature* of atmospheric winds, whereby stationary model predictions might overestimate AWC efficiency gains.

The present study focuses on the fluid mechanics relationship between the aerodynamics of a yawed rotor and the downstream deflection of the wake pattern, conditioned on the undisturbed

inflow mean *wind speed and turbulence intensity*. For this purpose we compare steady-state flow models - of various fidelities - mutually and with *full-scale* 2D flow fields reconstructed from long-range lidar (LRL) recordings. In order to facilitate, as close as possible, a one-to-one comparison, emphasis is given to select field data with small mean wind direction variations during the recording period.

2. Models

The flow models in question are a high-fidelity full non-linear CFD Reynolds-averaged Navier Stokes (RANS) solver, a medium-fidelity linear CFD RANS solver, and an augmented version of the Dynamic Wake Meandering (DWM) model. Considerations have been given to the potential effect of the WT rotational induction field (i.e. wake rotation) on wake deflection in cases of tilted rotor and/or sheared inflow conditions. With reference to Appendix A, this has been investigated using the non-linear CFD RANS solver, and only marginal effects from wake rotation are seen on down stream wake trace's. This is in line with previous investigations [4] showing only an negligible effect from wake rotation on power production of a downstream WT aligned with an upstream WT. The study detailed in Appendix A thus justifies neglecting wake rotation in the formulation of the simpler models investigated in this paper. The medium-fidelity CFD RANS solver can be generalised to include this effect, but only if second order perturbation terms are retained, meaning that the 'shortcut, introduced below for horizontally homogeneous fields, does not suffice. The augmented DWM approach cannot be extended to include wake rotation within the presented framework. For the present analysis, each of the three models describe downstream flow field cases behind a Vestas V52 WT, analogue to those reconstructed based on the LRL recordings.

2.1. RANS solver

The high-fidelity CFD RANS simulations of a single WT operating in yaw are carried out in EllipSys3D, which is an in-house finite volume flow solver, initially developed by Michelsen [5] and Sørensen [6]. The WT is placed on a flat rough surface, and the inflow represents a neutral atmospheric surface layer, where the roughness length is set by the ambient turbulence intensity based on the turbulent kinetic energy k, $I_k = \sqrt{2k/3}/\sqrt{u^2+v^2+w^2}$. The value of I_k is based on the measured streamwise I_u through $I_k = 0.8I_u$, which is derived from the standard ratios of turbulence components present in a neutral atmospheric surface layer, as described in previous work [7]. The rotor forces are modelled by an actuator disk (AD) using a generic force distribution including effects of shear and rotor rotation [8]. The RANS turbulence closure is based on an extended k-ε (two-equation) model [7] developed for WT wake simulations subjected to a neutral atmospheric surface layer. Denoting the rotor diameter by D, a cell spacing of $D/16$ around the AD is used in all three directions. Other details of the numerical domain can be found in van der Laan et al. [7]. The wake center, and thus the downstream wake trace, is obtained by fitting a one dimensional Gaussian profile to the streamwise velocity deficit at hub height.

2.2. Linearized RANS solver

The medium-fidelity linearized CFD RANS solver is the DTU in-house Fuga platform [9]. The governing Navier-Stokes equations are consistently linearized and conveniently formulated in a mixed spectral domain, which facilitates extremely fast solutions as based on a 'system' of look-up tables, where some are general and others are WT specific. These tables are subsequently used to determine the velocity field behind a single solitary WT. In analogy with the non-linear RANS approach, the drag from the rotor is modelled as an AD representing a uniform drag force.

In Fuga the Reynolds stresses are represented by a 'simple' eddy viscosity type of closure with the prescribed eddy viscosity $K = \kappa u_* z$, where κ denotes the von Karman constant. This simple closure works surprisingly well for wakes (better than standard $k-\varepsilon$ and mixing length closures). The model is described in in detail in [9] and [10]. Working also with the 'simple' closure, [11] found that the linearized version did not at all capture the effect of WT yaw misalignment. This observation is confirmed using Fuga results showing only a marginal yaw deflection, that even goes in the wrong direction. This behaviour can be understood by noting that the yaw deflection is basically *not* a first order effect. Writing the mean velocity as

$$(U, V, W) = (U_0, 0, 0) + (u, v, w),$$

where $U_0(z)$ is the horizontally uniform, unperturbed wind speed and (u, v, w) represent the wake. The term in the Navier-Stokes equation, which is responsible for wake deflection is $v\,\partial u_i/\partial y$, and, since this term is at least of second order, it is discarded during linearization. It would therefore seem that the modelling of yaw deflection using a linearized model is not possible. This is unfortunate, because very fast solvers can be made for linearized models. The principle of superposition, valid for solutions to linear equations, is particularly useful, because it means that the wake of a whole wind farm can be obtained by translating, rotating and scaling a pre-calculated solution for a singular, stand alone WT. Giving up linearity means that these features have to be sacrificed.

Linearization can be done in many ways, and the following variation seems to work for yaw deflection. For mathematical details confer [12]. The trick is to formulate the equations in curvilinear coordinates that vary along with the perturbation. In other words, we look at a stand alone WT and apply perturbation theory using the WT thrust coefficient, C_T, as a 'small' parameter. The first order equations are obtained by Taylor expanding u, v and w in powers of C_T and keep all terms proportional to C_T. Before that, however, a coordinate transformation of the form

$$(\acute{x}, \acute{y}, \acute{x}) = (x, y - \lambda, z),$$

is performed, where λ is an appropriate function of $\acute{x}$, $\acute{y}$ and $\acute{z}$ as well as C_T. The change of coordinates introduces new terms in the equations and alters the perturbation series depending on how we choose λ. It is natural to demand that $\lambda = 0$ for $C_\mathrm{T} = 0$, so that λ only contains first order terms or higher, and then it turns out that there are no 'extra' terms in the first order equations containing λ. This vanishing act is a result of the horizontal homogeneity and works regardless of chosen closure, but if we try to change the vertical z coordinate, setting $\acute{z} = z - \lambda_3$, then there will be first order terms containing λ_3. If we further demand that λ vanishes on the rotor disk, the first order problem (equations and boundary conditions) is not affected by λ in any way. This means that we can solve the linearized equations exactly as we would have done without the coordinate transformation without knowing the transformation. The only difference is therefore that the solution is formulated in the $\acute{x}\acute{y}\acute{z}$ coordinate system. However, going back to xyz, the solutions do depend on how λ is specified. Moreover, the λ reappear in the linearized equations, when they are expressed using x, y and z as independent variables. In particular the term $U_0 \partial u_i/\partial \acute{x}$, a linear remnant of the advection term, becomes

$$U_0 \frac{\partial u_i}{\partial \acute{x}} = U_0 \frac{\partial u_i}{\partial x} + U_0 \frac{\partial \lambda}{\partial \acute{x}} \frac{\partial u_i}{\partial y}$$

Since λ is at our disposal, we may choose it so that the extra term involving λ is equal to one of the second order terms that were discarded. This is achieved if we use

$$\lambda(\acute{x}, \acute{y}, \acute{z}) = \frac{1}{U_0(\acute{z})} \int_0^{\acute{x}} v(x', \acute{y}, \acute{z})\, \mathrm{d}x',$$

because then

$$U_0 \frac{\partial u_i}{\partial \acute{x}} = U_0 \frac{\partial u_i}{\partial x} + v \frac{\partial u_i}{\partial y}$$

Thus, the linear solution in $\acute{x}\acute{y}\acute{z}$ transforms to a solution to a nonlinear equation in xyz that contains the term $v\,\partial u/\partial y$, which is so crucial for yaw deflection.

It should be noted, that the solutions we have obtained with Fuga are not for a yawed actuator disk. The drag forces are smeared out in the x direction, so that the actuator 'disk' is more like an actuator 'sphere'. The same smeared out drag force distribution is used independent of yaw, except that direction of the force is turned according to the yaw. The solution can then be obtained for all yaw angles as a linear combination two solutions: one with purely longitudinal forcing, and one with purely transverse forcing. This dramatically speeds up calculations. Any external force field can be specified in Fuga including forces that make the wake rotate. However, like horizontal wake deflection, wake rotation is a second order effect, which Fuga, even in its revised form, would not be able to handle.

2.3. DWM Model

The WT yaw dictated wake deflection is a recent developed extension [13] to the 'classic' Dynamic Wake Meandering (DWM) model [14]. The wake deflection extension is based on the wake/ring-vortex analogy conjecture introduced in [15]. Rotational (induction) forces and mean wind shear are excluded, and, consistent with the 'classic' DWM model as well as the ring-vortex analogy, the wake deficit in the rotor plane is assumed circular symmetric in a vertical plane rotated the WT yaw angle, θ_y. The inflow to the yawed rotor is thus assumed uniform, however, with modified magnitude equal to $U_0 \cos\theta_y$, where U_0 denotes the uniform ambient wind speed in the mean wind direction. The wake/ring-vortex analogy is used to approximate the wake induced induction field. For this purpose, the Hill's vortex [16] is a convenient choice, because there exist a simple theoretically based relationship between the induced velocity of the ring vortex and the associated flow deficit *magnitude*. Thus

$$U_i(U_0, \theta_y, x) = -0.4\Delta U_w(U_0, \theta_y, x)$$

where $U_i(\cdot)$ is the induced velocity of the ring vortex flow structure, x is the downstream coordinate directed along the undisturbed mean wind direction, and $\Delta U_w(\cdot)$ is the wake deficit magnitude. The factor 0.4 follows directly from the mathematical formulation of Hill's vortex and is simply the ratio between the induced velocity of a Hill ring vortex system and the magnitude of the flow deficit resulting from the the same Hill ring vortex system as described in a coordinate system fixed to the Hill ring vortex system. The quasi-steady wake deficit, used in the 'classic' DWM model, is modelled as based on the thin layer approximation of the Navier-Stokes equations with the rotor aerodynamics consistently incorporated [17]. Navier-Stokes non-linearities are ignored, and *linear superposition* of the self-induced flow field of the organized flow structure representing the wake and the undisturbed ambient flow field is conjectured to suffice for the present purpose. Resolving the wake induction in fixed coordinates directed along the mean wind direction, U_a, and laterally, U_d, the laterally yaw dictated wake deflection, D_w, may be formulated as

$$D_w(U_0, \theta_y, x') = \int_0^{x'} \nabla_x D_w(U_0, \theta_y, x)\mathrm{d}x = \int_0^{x'} \frac{U_d(U_0, \theta_y, x)}{U_a(U_0, \theta_y, x)}\mathrm{d}x,$$

where ∇_x denotes the gradient operator with respect to the along wind direction x, and

$$U_a(U_0, \theta_y, x) = U_0 - 0.4\Delta U_w(U_0, \theta_y, x)\cos\theta_y,$$

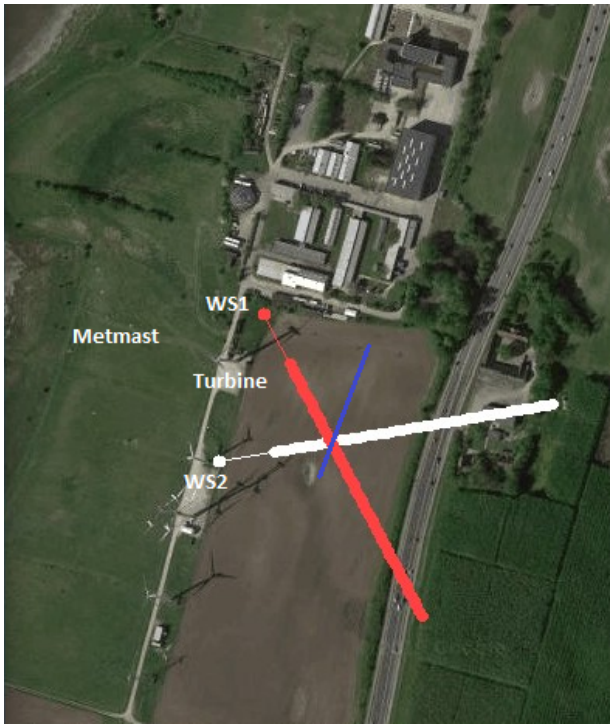

Figure 1: Overview of the setup used in the full-scale campaign. The white and red points depict an example of the coordinated measurement positioning of both lidar beams. The lidar beams are moved such that the intersecting point is always on the blue transect line.

$$U_d(U_0, \theta_y, x) = -0.4\Delta U_w(U_0, \theta_y, x) \sin \theta_y$$

To simulate the selected cases presented in Section 3, the rotor thrust's are selected identical for this model and the actuator disc's representing the models described in Sections 2.1 and 2.2.

3. Full-scale experiment

The full-scale demonstration was conducted at DTU's Risø test site located along the coast of Roskilde fjord. Two LRLs (described in [18]) were installed to resolve the flow field (2 components throughout a 3D volume) behind the DTU V52 test WT with high spatial resolution. The experimental setup is shown in Figure 1. The two LRLs were positioned on the ground approximately 50 m north of the turbine and 90 m south of the turbine, respectively. The scanning trajectory was designed such that the beams from the two LRLs were crossed following a set of three transect lines at various heights above the ground. Each transect was aligned perpendicular to the direction between the V52 WT and its upstream meteorological mast.

The scanners operated in dual-Doppler mode, where the positioning of both beams was synchronized along the three transect lines both in space and time. An example is illustrated by the blue line in Figure 1. The transect lines follow above-ground altitudes (agl) of 28 m, 54 m and 80 m, which are executed consecutively. The scanners are configured with multiple range-gates to measure along-beam distances from 50 m to 300 m with 5 m spacing. For a particular line-of-sight (LOS) this is illustrated in Figure 1 with the red and white points.

During the turbine test campaign, the V52 WT was operated with 3 sets of predefined/intended dynamic yaw errors (θ_y) for a variety of mean wind speeds: $\pm 10°$; $\pm 20°$; and $\pm 30°$. The recordings were based on one-hour runs and were designed in an attempt to

provide a best possible reference base case (i.e. zero yaw error) even under (moderately) varying inflow direction conditions. Figure 2 shows the yaw setting as a function of time. Between each yaw off-set a baseline case with zero yaw off-set was recorded.

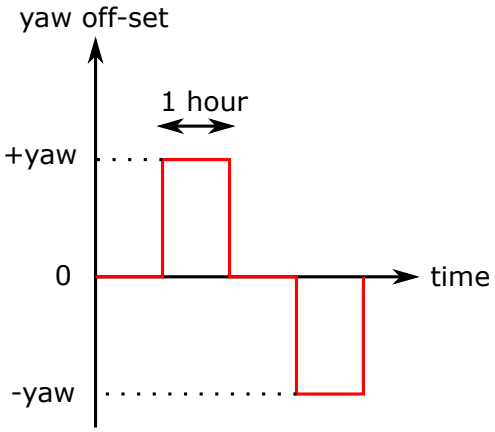

Figure 2: Yaw off-set shecual during test.

The test campaign resulted in two days of successful recordings - one day with mean wind speeds in the range 5-6 m/s, and one day with mean wind speeds ranging between 9 and 10 m/s. Both days only yaw off-set of $\pm 20°$ was recorded. For the analysis, it is important that populations 10-minute yaw cases, recorded under approximately identical conditions in terms of yaw error and mean wind speed, can be selected. This requirement is best satisfied for the 9-10 m/s campaign. For this day a case with positive, negative and zero yaw was selected and analysed. In each case multiple 10-min averages was chosen and averaged. In Figure 3 the yaw, wind direction and wind speed for the 10-min periods used in the analysis is shown. As expected, the field cases do not represent ideal stationary situations, and care has been taken to select 'sequences' as stationary as possible to facilitate the model-simulations comparisons best possible. The selected case studies, which are all associated with near-neutral atmospheric stability conditions, are summarised in Table 1. The positive yaw case is represented by the average of three 10-minute time series, the base (i.e. zero) yaw case is represented by the average of five 10-minute time series, and the negative yaw case is represented by the average of four 10-minute time series. The measured ambient turbulence intensity in Table 1 represents the streamwise turbulence intensity $I_u = \sigma_u/u$.

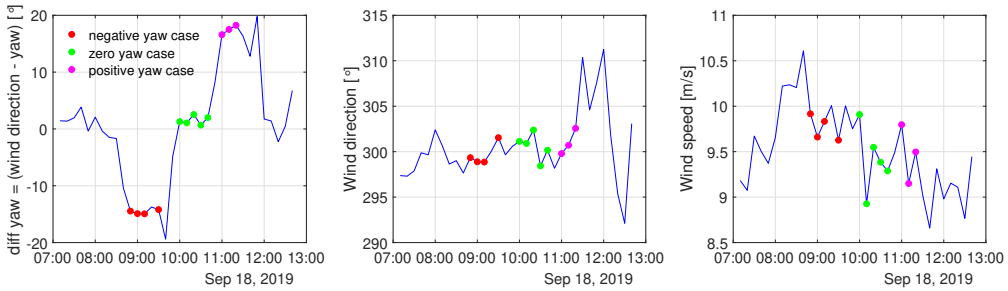

Figure 3: Ambient conditions for the experiment

Case	yaw misalignment [°]	I_u [%]	C_T	U_0 [m/s]
Zero yaw	1.51	6.20	0.83	9.41
Positive yaw	17.5	5.93	0.86	9.48
Negative yaw	-14.5	7.38	0.83	9.73

Table 1: Definition of test cases.

4. Analysis, Results and Discussion

The LOS wind speeds measured with the LRLs are interpolated on a 3D grid using a triangular-based linear interpolation. The grid size is 2 m × 2 m in the horizontal direction and 10 m in the vertical direction. For each 10-min period the xy-positions of the grid are rotated around the turbine position, so that the mean wind direction is parallel with the x-axis. The rotated 10-minute data sets are then averaged over longer periods, where the induced yaw difference and environmental conditions are approximately similar. For the plot (see Figures 4-6) the x- and y-axis are normalised with the rotor diameter, and the (0,0) reference point is the position of the turbine.

The interpolated LOS wind speeds from each scanner are combined to give the *horizontal* wind speed using the method described in [19]. In this method it is assumed that the vertical wind component, w, can be neglected. This assumption is valid if the terrain is very flat, and if the elevation angle of the lidar beam is very small. For this experiment the latter is not valid, since the beams has elevation angle of up to about 40 degrees in order to reach hub-height. For the cases analysed in this paper the wind direction has been from north-west, and for these wind direction the wind is coming from fjord nearby. From this direction the terrain is flat, however, with a slope up to the turbine.

A horizontal plane of the wind field is shown at hub-height in Figures 4-6. Each of these figures illustrates the wake affected flow field behind the WT reconstructed from the lidar measurements as well as the same flow field predicted by the three models described in Section 2.

In the investigated horizontal plane the wake-centre position is estimated by a least-square 1D Gaussian fit cross section of the wake in the cross wind direction. The Gaussian fit turned out to work well as a measurement 'noise' reduction filter. Prior to the Gaussian fit, the wake of the lidar data is isolated by filtering out high wind speeds above $1.1U_0$. The resulting measured wake trace's is illustrated by the 'magenta' curves on the plots. All of these display the expected wake deflection in the near wake regime, but a contra-intuitive behaviour longer down stream, where the wake seems to 'bend' southwards. This behaviour is consistent in that it shows up in all the three investigated cases.

The aim of the present analysis is to investigate the effect of provoked WT yaw errors on the down stream wake trace's. Therefore, to eliminate the contra-intuitive behaviour of the wake deflection pattern at longer down stream distances and thus to isolate the yaw effect on the wake trace's, it was decided to use the zero-yaw case as the deflection base case, and measure the effects of the provoked WT yaw settings relative to this base case. The result is shown in Figure 7, where the wake trace's, relative to the base case, are plotted as function of downstream distance for both measurements and simulations. The measurements compare very well with the CFD RANS simulations, whereas the two more simple models, in the investigated two cases, overestimate the wake deflection by about a factor of two.

The fact that these two models give almost identical results is remarkable, as they are quite different although both based on first principles - Fuga being based on a solution of the linerized set of Navier-Stokes equations, and Hill's vortex ring system being based on a solution to the non-linear Euler equations (i.e.Navier-Stokes equations with zero viscosity). Despite these differences in origin, the resulting induction fields are quite similar.

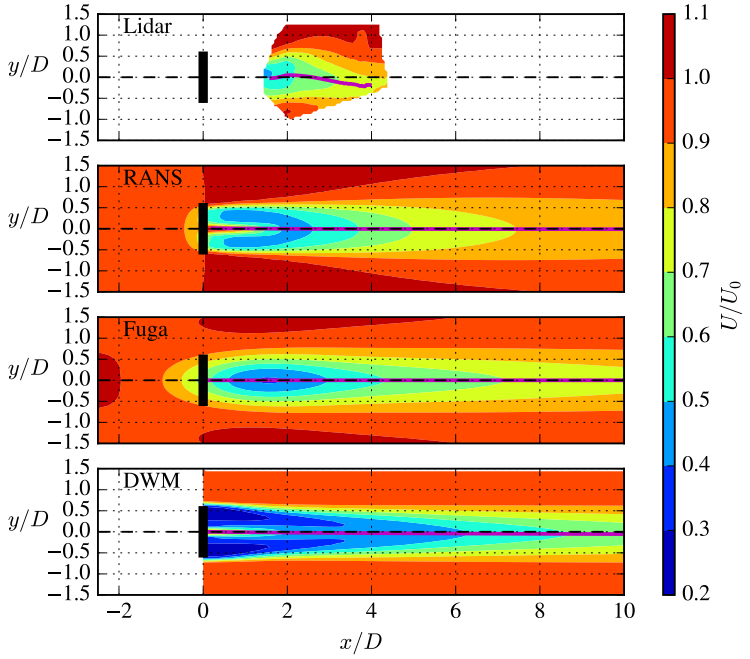

Figure 4: Zero yaw case: Measured and modelled streamwise velocity normalized by U_0. Derived wake center is shown by magenta line. Wind turbine is illustrated by the black rectangle.

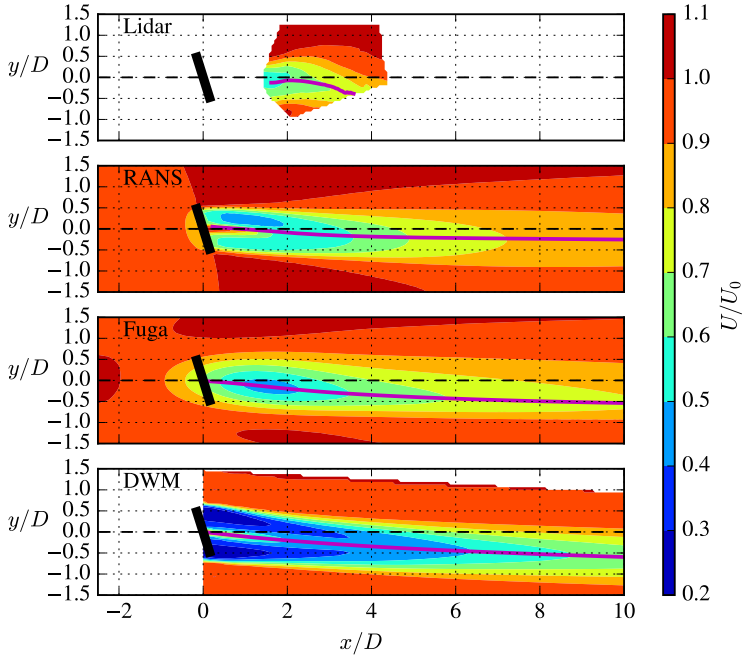

Figure 5: Similar to Figure 4 for the positive yaw case.

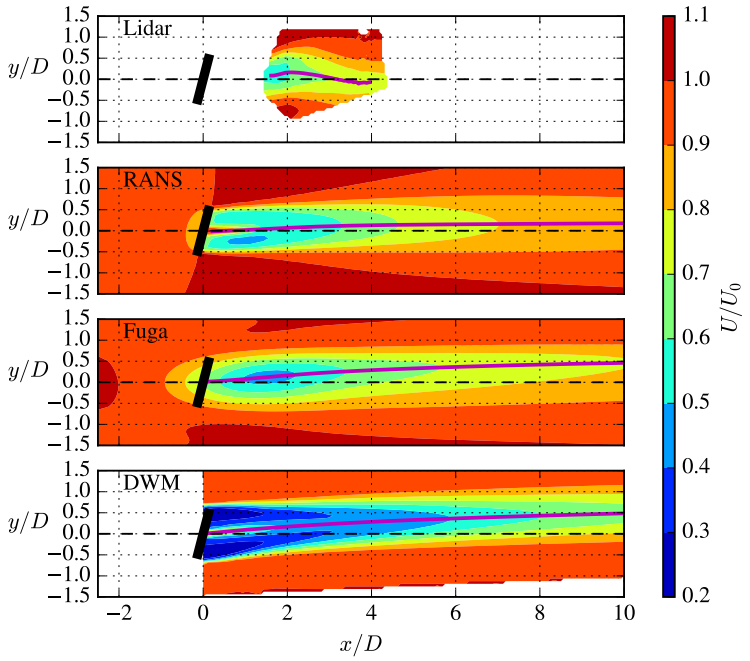

Figure 6: Similar to Figure 4 for the negative yaw case.

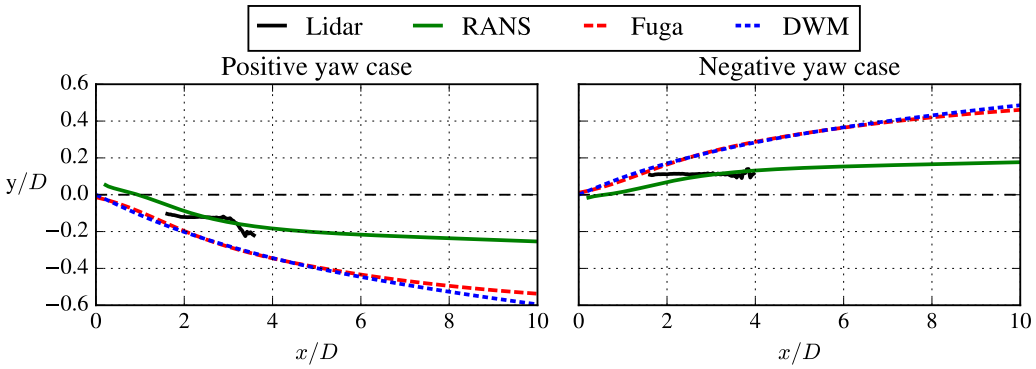

Figure 7: Wake center lines derived from lidar data and flow models. Lidar wake center lines represent the difference between a non-zero and the zero yaw case.

5. Conclusion

A popular strategy used for wind farm control is based on active WT yaw control, where the wake is deflected with the purpose of mitigating wake effects on nearby downstream located wind turbines. This is still an active area of research, and there is a need to consolidate model predictions by comparing with full-scale flow measurements.

In this paper, we compare predictions from three models - of various fidelities - with reconstructed flow fields based on a dedicated lidar campaign using two long range lidars operated in dual-Doppler mode. The lidar campaign was running for three days, and to the knowledge of the authors, this is the first time a horizontal slices of wake trace's have been resolved full-scale. Ideally, stationary wind conditions are requested, but due to the stochastic

nature of wind flow fields this is an abstraction that hardly is achievable. Consequently, 10-minute sequences with approximately identical flow characteristics were averaged and used in the comparative analysis. An additional unexpected challenge appeared in the reconstructed full-scale flow fields - namely a contra-intuitive behaviour of the the of the wake in the far wake regime where the wake bend to the right even for the zero-yaw case. This phenomenon is present in all measurements, and is conjectured to affect the downstream wake trace's. Therefore, the WT yaw effect of the wake pattern is investigated with reference to the zero-yaw base case, thus isolating the yaw effect on wake deflection.

Two yaw cases were investigated, characterized by yaw errors of respectively $17.5°$ and $-14.5°$. The measurements show good agreement with CFD RANS simulations, whereas the two more simple models, in the investigated two cases, overestimate the wake deflection by about a factor of two. In a future perspective more cases must be investigated before final conclusions can be made, preferable including detailed inflow recordings as well as 'dry runs', where the investigated WT is stopped between the different yaw settings to provide characteristics of the flow conditions at the investigated site without the presence of an operating WT.

Acknowledgements

Acknowledgements This research was partly supported by the Danish PowerKey project (EUDP Project No. 12558) and partly by the EU Horizon 2020 research and innovation program, under grant agreement no. 727680 (TotalControl). The authors would also like to recognize efforts by the technical staff at Risø for carrying out the wind turbine control tests.

References

[1] Vitulli J, Larsen G C, Pedersen M, Ott S and Friis-Møller M 2019 *Journal of Physics: Conference Series* vol 1256 (IOP Publishing) p 012027
[2] Kanev S, Savenije F and Engels W 2018 *Wind Energy* **21** 488–501
[3] Kheirabadi A C and Nagamune R 2019 *Journal of Wind Engineering and Industrial Aerodynamics* **192** 45–73
[4] van der Laan M P, Sørensen N N, Réthoré P E, Mann J, Kelly M C, Troldborg N, Hansen K S and Murcia J P 2015 *Wind Energy* **18** 2065
[5] Michelsen J A 1992 Basis3d-a platform for development of multiblock pde solvers Tech. rep. Technical Report AFM 92-05, Technical University of Denmark
[6] Sørensen N N 1995 *General purpose flow solver applied to flow over hills* vol 827 (Risø National Laboratory Roskilde)
[7] van der Laan M P, Sørensen N N, Réthoré P E, Mann J, Kelly M C, Troldborg N, Schepers J G and Machefaux E 2015 *Wind Energy* **18** 889
[8] Sørensen J N, Nilsson K, Ivanell S, Asmuth H and Mikkelsen R F 2020 *Renewable Energy* **147** 2259
[9] Ott S, Berg J and Nielsen M 2011 Linearised cfd models for wakes Tech. rep. Danmarks Tekniske Universitet, Risø Nationallaboratoriet for Bæredygtig Energi
[10] Ott S and Nielsen M 2013 Developments of the offshore wind turbine wake model fuga Tech. Rep. DTU Wind Energy, report E–0046 Danish Technical University URL `http://www.wasp.dk/Fuga`
[11] Peters C 2018 A linearized approach to wind turbine aerodynamics Tech. Rep. Ph. D. thesis 951027-T225 Royal Institute of Technology, KTH Mechanics
[12] Ott S, van der Laan P and Larsen G C 2019 Upgrade of fuga Tech. Rep. DTU Wind Energy Danish Technical University deliverable D1.7 of the TotalControl Project
[13] Larsen G C, van der Laan P and Andersen S J 2019 Upgrade of the dynamic wake meandering model Tech. Rep. DTU Wind Energy Danish Technical University deliverable D1.6 of the TotalControl Project
[14] Larsen G C, Madsen H A, Thomsen K and Larsen T J 2008 *Wind Energy* **11** 377–395
[15] Machefaux E, Larsen G C, Troldborg N, Gaunaa M and Rettenmeier A 2015 *Wind Energy* **18** 2085–2103
[16] Akhmetov D G 2009 *Vortex Rings* (Springer: Berlin Heidelberg)
[17] Madsen H A, Larsen G C, Larsen T J, Troldborg N and Mikkelsen R F *Journal of Solar Energy Engineering* **132**
[18] Vasiljević N, Lea G, Courtney M, Cariou J P, Mann J and Mikkelsen T **8** 896 URL `https://www.mdpi.com/2072-4292/8/11/896`
[19] A comparison of sector-scan and dual doppler wind measurements at høvsøre test station – one lidar or two?

Appendix A. Effect of rotor rotation on wake deflection based on RANS

Additional RANS simulations of an AD without rotor rotation are performed for all three yaw cases (as defined in Table 1). The rotor rotation is switched off by setting the tangential forces to zero. The wake center line is derived from each RANS simulation using a Gaussian fit of the wake deficit at hub height, and the results are depicted in Figure A1. For zero yaw misalignment angle, the rotor rotation deflects the wake counter clockwise, as seen from above. The rotor rotation reduces the wake deflection for a negative yaw misalignment angle, while it increases the wake deflection slightly for a positive yaw misalignment angle. The difference of the wake center due to rotor rotation is depicted in the right plot of Figure A1, and it indicates that the rotor-rotation-induced wake deflection is between -2% and 1% for a downstream distance of 2-10D.

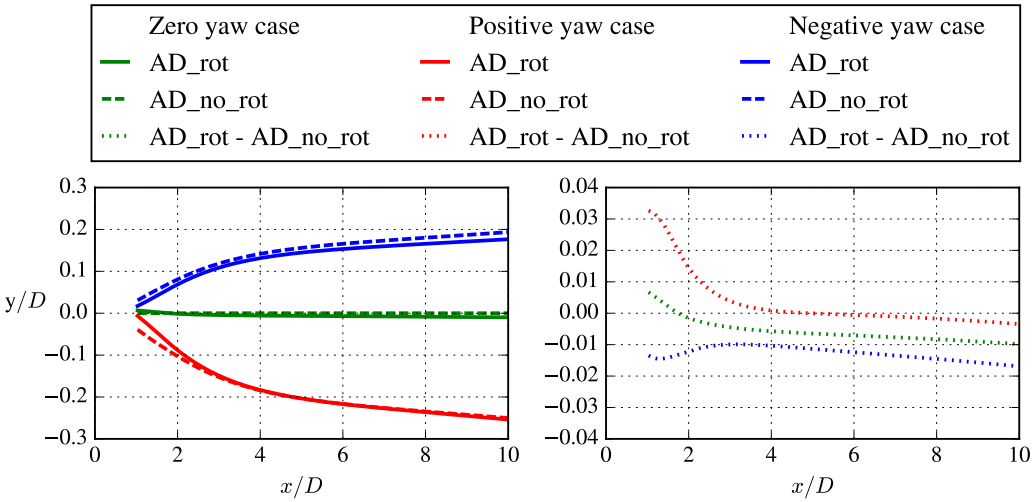

Figure A1: Left plot: Wake center lines derived from RANS simulations, with and without rotor rotation. Right plot: Effect of rotation on the wake center line.